Volume 7
Number 11
November 2020
Pages 3205–3630

Environmental Science Nano

rsc.li/es-nano

ISSN 2051-8153

ROYAL SOCIETY OF CHEMISTRY

PAPER

Mohammed Baalousha *et al.*

Nanoparticle size and natural organic matter composition determine aggregation behavior of polyvinylpyrrolidone coated platinum nanoparticles

Environmental Science Nano

ROYAL SOCIETY OF CHEMISTRY

PAPER

View Article Online
View Journal | View Issue

Cite this: *Environ. Sci.: Nano*, 2020, 7, 3318

Nanoparticle size and natural organic matter composition determine aggregation behavior of polyvinylpyrrolidone coated platinum nanoparticles†

Mithun Sikder, [a] Jingjing Wang,[a] Brett A. Poulin, [bc] Malak M. Tfaily[de] and Mohammed Baalousha *[a]

Received 23rd June 2020,
Accepted 22nd September 2020

DOI: 10.1039/d0en00659a

rsc.li/es-nano

Engineered nanoparticle (NP) size and natural organic matter (NOM) composition play important roles in determining NP environmental behaviors. The aim of this work was to investigate how NP size and NOM composition influence the colloidal stability of polyvinylpyrrolidone coated platinum engineered nanoparticles (PVP-PtNPs). We evaluated PVP-PtNP aggregation as a function of the NP size (20, 30, 50, 75, and 95 nm, denoted as PVP-PtNP$_{20-95}$) in moderately hard water (MHW). Further, we quantified the effect of the hydrophobic organic acid (HPOA) fraction of NOM on the aggregation of PVP-PtNP$_{20}$ and PVP-PtNP$_{95}$ using 6 NOM samples from various surface waters, representing a range of NOM compositions and properties. NOM samples were characterized for bulk elemental composition (*e.g.*, C, H, O, N, and S), specific ultraviolet absorbance at 254 nm (SUVA$_{254}$), and molecular level composition (*e.g.*, compound classes) using ultrahigh resolution mass spectrometry. Single particle-inductively coupled plasma-mass spectrometry (sp-ICP-MS) was employed to monitor the aggregation of PVP-PtNPs at 1 μg PVP-PtNP per L and 1 mg NOM per L concentrations. PVP-PtNP aggregate size increased with decreasing primary PVP-PtNP size, likely due to the lower zeta potential, the higher number concentration, and the higher specific surface area of smaller NPs compared to larger NPs at the same mass concentration. No aggregation was observed for PVP-PtNP$_{95}$ in MHW in the presence and absence of the different NOM samples. PVP-PtNP$_{20}$ formed aggregates in MHW in the presence and absence of the six NOM samples, and aggregate size increased in the presence of NOM likely due to interparticle bridging of NOM-coated PVP-PtNPs by divalent counterions. PVP-PtNP$_{20}$ aggregate size increased with the increase in NOM elemental ratio of H to C and the relative abundance of lignin-like/carboxyl rich-alicyclic molecules (CRAM)-like compounds. However, the aggregate size of PVP-PtNP$_{20}$ decreased with the increase in NOM molecular weight, NOM SUVA$_{254}$, elemental ratio of O to C, and the relative abundance of condensed hydrocarbons and tannin-like compounds. Overall, the results of this study suggest that the composition and sources of NOM are key factors that contribute to the stability of PVP-PtNPs in the aquatic environment.

Environmental significance

This study provides insights on the aggregation of polyvinylpyrrolidone coated platinum nanoparticle (PVP-PtNP) based on PVP-PtNP primary particle size and the molecular properties of natural organic matter (NOM). The aggregate size of PtNP increased with decreasing primary PVP-PtNP size. 20 nm PVP-PtNP (PVP-PtNP$_{20}$) formed aggregates in the presence and absence of the same NOM samples, and aggregate size increased in the presence of NOM. The aggregate size of PVP-PtNP$_{20}$ (1) increased with increasing NOM elemental ratio of H to C and the relative abundance of lignin-like compounds/carboxyl rich alicyclic molecules, and (2) decreased with increasing NOM molecular weight, SUVA$_{254}$, elemental ratio of O to C, and the relative abundance of condensed hydrocarbon and tannin-like compounds. These results reveal that the molecular properties of NOM, and thus composition and sources, are key factors that contribute to the stability of PtNPs in the aquatic environment.

[a] *South Carolina SmartState Center for Environmental Nanoscience and Risk (CENR), Department of Environmental Health Sciences, University of South Carolina, 921 Assembly Street, Columbia, SC, 29208, USA. E-mail: mbaalous@mailbox.sc.edu; Tel: +1 803 777 7177*
[b] *U.S. Geological Survey, Boulder, CO, 80303, USA*
[c] *Department of Environmental Toxicology, University of California Davis, Davis, CA 95616, USA*
[d] *Environmental Molecular Sciences Laboratory, Richland, WA 99354, USA*
[e] *Department of Environmental Science, University of Arizona, AZ 85721, USA*
† Electronic supplementary information (ESI) available. See DOI: 10.1039/d0en00659a

Introduction

The colloidal stability of engineered nanoparticles (NPs) has been studied extensively over the past two decades. Numerous studies measured NP aggregation for different types of NPs with a major focus on investigating the effect of NP surface coating, media ionic strength, ion valency, and natural organic matter (NOM).[1,2] Yet, there is a limited and often contradictory knowledge on the effect of both NP size and NOM properties on the aggregation of NPs. For instance, whereas some studies reported a decrease in the critical coagulation concentration (CCC, the minimum counterion concentration required to fully destabilize the dispersion) with the decrease in NP size (*e.g.*, hematite,[3] TiO_2 (ref. 4)), others reported an increase in CCC with the increase in NP size (*e.g.*, CdSe NP[5]) or an independence of CCC and NP size (*e.g.*, AuNPs,[6] AgNPs,[2] PtNPs[7]). Further, some studies reported a positive linear correlation between the CCC and NP size (*e.g.*, anatase TiO_2 (ref. 4)), while others found that the CCC correlated better with NP specific surface area (*e.g.*, TiO_2,[4] CdSe NP[5]), and another study reported no correlation between CCC and NP size and/or specific surface area in the presence of monovalent and divalent electrolytes (*e.g.*, PtNPs[7]).

NOM is ubiquitous in the environment with concentrations in major rivers commonly between 1 to 10 mg-C per L, depending on biochemical and climatic conditions.[8–10] NOM is a complex mixture of polyelectrolytic and polyfunctional organic molecules (*e.g.*, polysaccharides, proteins, lipids, nucleic acids, and fulvic and humic substances)[11,12] that vary spatially and temporally in terms of molecular composition, acidity, molecular weight, structure, and charge density.[13] The adsorption of NOM on NP surfaces[14] results in the formation of an NOM-corona,[15] giving NPs a unique surface identity, which may determine the environmental behavior of NPs. NOM can act as a competitor to displace intentional engineered coatings (*e.g.*, citrate, polyvinylpyrrolidone, PVP) on NPs. For instance, NOM molecules (*i.e.*, both humic and fulvic acids) can displace citrate coatings from the surfaces of AgNPs[16] and AuNPs[17] due to the higher affinity of NOM molecules for NP surfaces. Model thiol ligands (*e.g.*, cysteine) can replace the PVP coating on AgNPs,[18] which suggests that thiol groups present in NOM may play an important role in determining NOM interfacial interactions with PVP-coated NPs. NOM can enhance NP stability by enhancing NP electrostatic repulsion and/or steric hindrance.[19–21] However, the impact of NOM on the environmental behaviors of NPs depends on the properties of NOM such as charge density, functional groups, and molecular weight.[22] For instance, higher molecular weight NOM increases the stability of AuNPs due to increased electrosteric repulsion.[22–25] The aggregation of ZnS NPs decreased with increasing NOM concentration, the molecular weight and aromatic content of NOM fractions, while the carboxylate and reduced sulfur content of NOM had little effect.[26]

Recently, the application of ultrahigh resolution mass spectrometry, specifically Fourier transform-ion cyclotron resonance-mass spectroscopy (FT-ICR-MS), to natural matrices has offers resolving power sufficient to identify the molecular formulas of thousands of unique molecules that make up NOM. FT-ICR-MS measures the mass-to-charge ratio of organic molecules with up to six decimal place precision,[27] and allows the discrimination of compositional differences between different NOM samples. Similarly, recent developments in single particle inductively coupled plasma mass spectrometry (sp-ICP-MS) allows measuring NP size and aggregation at environmentally relevant NP concentrations.[28] Such measurements and understanding have been limited by the detection limits of commonly implemented analytical techniques for NP sizing and aggregation such as dynamic light scattering (DLS) and nanoparticle tracking analysis (NTA). These methods require high NP concentrations, typically in the mg L^{-1} range,[29] which is well above the predicted environmental concentrations of most NPs (*e.g.*, ng L^{-1} to μg L^{-1}).[30,31] At such high concentrations, NPs aggregate at faster rates, form larger aggregates, are more likely to settle out of solution, and dissolve at slower rates.[32] Together, data obtained by FT-ICR-MS on NOM molecular composition and by sp-ICP-MS on NP aggregation, will advance the understanding of the changes in NP aggregation that are associated with changing NOM conditions (*e.g.*, concentrations and molecular composition) under environmentally relevant low NP concentrations.

The release of platinum into the environment has increased due to widespread use in automobile catalysts[33–38] and some studies demonstrated that the release of Pt in road dust is in the form of nanoparticles.[39] The expected Pt concentration is 0.4–10.8 ng L^{-1} in aquatic ecosystems and 50 ng kg^{-1} in the road dust.[40] The occurrence of PtNPs in the environment raises concerns regarding the potential environmental implications (*e.g.*, bioaccumulation and/or toxicity) of PtNPs.[41] Several studies reported bioaccumulation and toxicological effects of Pt in aquatic organisms, such as water fleas,[42] freshwater oligochates,[43] microalgae,[44] and marine bacteria.[45]

The aims of this study were to determine the impacts of 1) the primary particle size of NPs, and; 2) the properties and the molecular composition of the hydrophobic organic acid (HPOA) fraction of NOM on the aggregation behavior of PVP-PtNPs at environmental relevant NP concentrations using state-of-the-art analytical techniques of sp-ICP-MS and FT-ICR-MS.

Methodology

NP synthesis

Polyvinylpyrrolidone coated platinum engineered nanoparticles (PVP-PtNPs) were synthesized according to the approach described by Sikder *et al.* (2018).[7] First, citrate coated platinum engineered nanoparticles (cit-PtNPs) of different sizes (*e.g.*, 10, 17, 31.6, 59.3, 53.5 nm, measured by DLS) were synthesized using seed-mediated growth approach as described elsewhere.[7] Second, PVP-PtNPs ($PtNP_{20}$, $PtNP_{30}$, $PtNP_{50}$, $PtNP_{75}$, $PtNP_{95}$) were obtained by a ligand exchange approach using cit-PtNPs as precursors. Briefly, 300 mL cit-

PtNPs of different sizes (*e.g.*, 10, 17, 31.6, 59.3, 53.5 nm) were converted into PVP-PtNPs by adding 1.0, 0.85, 0.48, 0.20, and 0.12 mL of 7.7 mM PVP solution, respectively, under vigorous stirring (700 rpm) for at least 1 h. The PVP amount selected was that required to obtain a surface coverage of 8 PVP molecules nm^{-2} according to the method presented elsewhere.[7] PVP coating was used to obtain stable engineered nanoparticles with uniform size distributions.[46] Additionally, PVP coating was used as a model coating because it is one of the widely used capping agent in the synthesis of engineered nanoparticles allowing comparison to other studies.

Nanoparticle characterizations

The core size and morphology of the synthesized PVP-PtNPs ($PtNP_{20}$–$PtNP_{95}$) were measured using transmission electron microscopy (TEM, LaB_6 Jeol 2100, 200 KeV, MA, USA). Samples for TEM analysis were prepared by depositing a droplet of undiluted PVP-PtNP suspension on a 300-mesh carbon coated Cu-grid (Agar Scientific, Stansted, UK) for 15 min followed by rinsing with ultra-pure water (UPW). The grids were then left to dry at room temperature for 48 h in a covered petri dish. The elemental composition of the synthesized PVP-PtNPs was confirmed by energy dispersive X-ray spectroscopy (EDS, Jeol EX-230 silicon drift detector, MA, USA) coupled with the TEM. Particle size was measured using the Gatan Digital Micrograph software package (GMS 3).[47] At least 150 individual NPs were analyzed to determine the particle size distribution (PSD) and the mean size. The *z*-average hydrodynamic diameter (Z_{avg}), polydispersity index (PDI), and electrophoretic mobility of the synthesized PVP-PtNPs were determined by dynamic light scattering (DLS) and laser Doppler electrophoresis using a Zetasizer Nano-ZS instrument (Malvern Instruments Ltd., MA, USA). The Z_{avg} and zeta potential were determined only at high particle concentrations (>1 mg L^{-1}), where robust zeta potential measurements were obtained. The theoretical particle number concentration of 1 μg L^{-1} PVP-PtNPs was calculated by dividing the mass concentration by the average primary particle mass, which was calculated using particle density (21.45 g cm^{-3}) and diameter as measured by TEM.

NOM samples

The HPOA fraction of NOM was isolated from a wide range of aquatic environments (details in Table S1†) including: three saw-grass dominated wetlands in the northern Florida Everglades Water Conservation Area (WCA) 2A at site F1 (NOM 1), WCA 2B South (NOM 2), and Arthur R. Marshall Loxahatchee National Wildlife Refuge (LOX) at site 8 (NOM 6); the Suwannee River (Georgia; NOM 5), Williams lake (Minnesota; NOM 3); and Pacific Ocean surface water near Hawaii (NOM 4). The HPOA fraction of NOM was isolated on XAD-8 resin,[48] which is a chemically distinct NOM fraction that is recognized as reactive to natural[49] and engineered NPs[50] and is a suitable fraction of NOM to represent the most influential NOM molecules in natural waters. NOM samples were freeze-dried immediately after isolation to minimize NOM alternation prior to NP stability experiments. Additional details on the isolation of the Everglades[51] and Pacific Ocean samples[52] are available elsewhere. Solid-phase extraction is obligatory for the NOM analyses made in this study and experiments with NPs. Specifically, the solid-phase extraction produces a salt-free extract that is necessary for FTICR-MS analysis. Further, the use of salt-free NOM samples in NP stability experiments allows experiments to be performed under the identical aqueous conditions (*i.e.*, not influenced by inorganic ions from the different NOM samples). Isolation of NOM by solid-phase extraction on XAD resins and use of alkaline solution is the method recommended by the International Humic Substances Society. Properties of NOM samples including the bulk elemental compositions (C, H, O, N, S) and specific ultraviolet absorbance at 254 nm ($SUVA_{254}$) are provided in Table S1.†[53,54]

Molecular characterization of NOM using FT-ICR-MS

NOM samples were reconstituted directly in HPLC-grade methanol at a concertation of 20 mg L^{-1} and analyzed by FT-ICR-MS by direct injection in negative ionization mode. A 12 Tesla Bruker Solarix FT-ICR-MS located at the Environmental Molecular Sciences Laboratory in Richland, WA, was used to collect ultrahigh-resolution mass spectra of the NOM samples. A standard Bruker electrospray ionization (ESI) source was used to generate negatively charged molecular ions. Samples were introduced directly to the ESI source at a flow rate of 3 μL min^{-1}. The ion accumulation time was varied, from 0.1 to 0.5 s, to account for differences in carbon (C) concentration between samples. The instrument was externally calibrated weekly with a tuning solution from Agilent (Santa Clara, CA), which calibrates to a mass accuracy of <0.1 ppm. Two hundred scans were averaged for each sample and internally calibrated using the homologous series of organic molecules separated by 14 Da ($–CH_2$ groups). The mass measurement accuracy was less than 1 ppm for singly charged ions across a broad m/z range (*i.e.*, $200 < m/z < 1200$). To further reduce cumulative errors, all sample peak lists for the entire dataset were aligned to each other prior to formula assignment to eliminate possible mass shifts that would impact formula assignment. Putative chemical formulas were assigned using Formularity software.[55] Chemical formulas were assigned based on the following criteria: signal to noise ratio (S/N) >7, and mass measurement error <1 ppm, taking into consideration the presence of C, H, O, N, S and P and excluding other elements. Peaks with large mass ratios (m/z values >500 Da) were assigned formulas through the detection of homologous series (CH_2, O, H_2). Additionally, to ensure consistent assignment of molecular formulas, the following rules were implemented: one phosphorus requires at least four oxygens in a formula, and when multiple formula candidates were assigned the formula with the lowest error and with the lowest number of heteroatoms was picked. The molecular

formulas were grouped based on heteroatom composition: CHO, CHON, CHOS, CHOP, CHONS, CHONP, and CHONSP. Further, the molecular formulas were also tentatively grouped into eight compound classes based on elemental stoichiometries: condensed aromatic compounds, unsaturated hydrocarbons, tannins, lignin/carboxyl-rich alicyclic molecules (CRAM), lipids, proteins, amino sugars, and carbohydrates (according to Tfaily *et al.* 2015)[56] (criteria detailed in Table S2†). It is important to note that CRAM fits within the van Krevelen space labeled "lignin-like". Assignments of molecular formulas to compound classes are tentative because structural information cannot be gained from molecular stoichiometries alone. Additional analysis is required to tease apart whether lignin and/or CRAM exist in the samples. As such, we included both identifications in the discussion. From the formula assignment, the average (by number-weighted) abundance of each class was calculated and compared between samples.[56] The relative abundance of molecules based on heteroatom content and compound classification are presented in Tables S3 and S4,† respectively. The molecular properties (*e.g.*, molecular weight, O/C, and O/H) of the NOM samples were calculated from the assigned molecular formulas and are summarized in Table S5.†

Aggregation of PVP-PtNPs

The aggregation behavior of PVP-PtNPs ($PtNP_{20}$–$PtNP_{95}$) was determined by monitoring the evolution of PVP-PtNP number size distribution and number and mass concentrations by sp-ICP-MS after (*e.g.*, 0 and 24 h) mixing 1 μg L^{-1} PVP-PtNPs with UPW and moderately hard water (MHW; composition detailed in Table S6†). The effect of NOM on the aggregation of PVP-PtNPs in MHW was determined after mixing 1 μg L^{-1} PVP-PtNPs ($PtNP_{20}$ and $PtNP_{95}$) with MHW in the presence of 1 mg L^{-1} NOM under static conditions. All aggregation experiments were conducted in triplicate. We present the average of experimental triplicate measurements for the number and mass concentrations and the number-average diameter values. All sp-ICP-MS data were acquired with a NexION™ 350D ICP-MS (PerkinElmer Inc., MA, USA) operating in a single particle mode with the Syngistix Nano Application Module. A standard introduction system was used consisting of a Meinhard glass concentric nebulizer, a glass cyclonic spray chamber, and a 2 mm inner-diameter quartz injector. The sample uptake rates were 0.28–0.32 mL min^{-1}. Data were acquired at an RF power of 1600 W, a 50 μs dwell time, a 0 μs settling time, and a 60 s acquisition time. The transport efficiencies were 9.6–12.7%. NIST™ Au standard reference material (actual TEM size of 56 nm; reference material 8013 manufactured by National Institute of Standard and Technology, MD, USA) was used to determine the transport efficiency. A rinse cycle, consisting of 1 min with 1% *aqua regia* and 1 min with UPW, was performed after each sample run to ensure cleansing of the sample introduction system between samples. The NIST Au standard reference material was measured after each set as a QA/QC check.

Statistical analysis

Statistical analyses were performed with SAS® version 9.4 software (SAS institute, Cary, NC). Correlation coefficients between the percentage of mass of aggregated NPs and the NOM elemental composition and properties were calculated using Pearson's correlation method. Calculated Pearson's correlation coefficient (r) and p-values (Table 1) were used to assess the correlation quality with each NOM parameter. The percentage of mass of aggregated NPs in the presence of six NOM samples and a control (without NOM) were analyzed using ANOVA and Tukey's multiple comparison test. Particle size distribution of PVP-PtNPs in the absence and presence of different NOM samples were analyzed using Kolmogorov–Smirnov (K–S) test with Bonferroni correction. In all cases, the statistical significance was set at p-value <0.05.

Results and discussions

NOM characterization

The number-average molecular weight and $SUVA_{254}$ values of the HPOA fractions of NOM samples varied between 369–442 Da and 0.8–4.8 L mg^{-1} m^{-1}, respectively (Tables S1 and S6†). The N and S content of the NOM samples varied significantly (0.8–1.8% and 0.4–1.9%, respectively, Table S1†). CHO and CHON were the main classes of compounds when grouped by heteroatom composition (>5% of total formulas), and displayed a notable variation between the six NOM samples (Table S3†). CHOS and CHONS were generally less abundant (1.6 to 7.5% and 1.9 to 8.1% of total formulas, respectively) with select NOM samples (NOM 1, 2 and 5) containing > 5% of these two classes of compounds, and the abundance of these formulas largely following elemental S and N content (Table S1†). Heteroatom classes of compounds including P (*e.g.*, CHOP, CHONP, CHONSP, and others) represented only <5% of all formulas in all NOM samples. Condensed

Table 1 Analysis results of Pearson's correlation between aggregated $PtNP_{20}$ mass and NOM properties

Variables	Pearson's correlation coefficient (r)	p-Value
% mass of aggregated NP *vs.* NOM elemental composition		
O	−0.411	0.418
N	−0.164	0.756
S	−0.429	0.397
$SUVA_{254}$	−0.771	0.072
Molecular weight	−0.979	0.004[a]
O/C	−0.841	0.036[a]
H/C	0.730	0.099
% mass of aggregated NP *vs.* NOM formula assignments by compound classes		
Aminosugar	0.709	0.115
Condensed HC	−0.766	0.076
Carbohydrates	−0.746	0.089
Lignin	0.798	0.058
Lipid	0.409	0.420
Protein	0.748	0.087
Tannin	−0.898	0.015[a]
Unsaturated HC	−0.171	0.745

[a] Inidicates correlations with stastical sinigificnce.

hydrocarbon-, lignin-/CRAM-, and tannin-like compounds were the main chemical classes of compounds in NOM and varied significantly between the six NOM samples (Table S4†). Other molecules assigned to compound classes (*e.g.*, aminosugar, carbohydrates, lipid, unsaturated hydrocarbons, and others) represented <5% of all formulas in all NOM samples. It is important to recognize that the type of sorbent used for solid-phase extraction of NOM influences the molecular diversity as determined by FTICR-MS.[57] The number average elemental ratio of O/C and H/C varies within a narrow range (0.48–0.52 and 1.05–1.26, respectively, Table S5†) between the different NOM samples. Collectively, the observed differences in the bulk elemental composition, $SUVA_{254}$, and molecular properties of NOM samples reflect differences in NOM source and environmental processing (Table S1†), rather than ionization and detection variations in the measurement technique as all samples were analyzed using the same protocol and at the same time.

Particle characterization

TEM micrographs show that the synthesized PVP-PtNPs are spherical (Fig. S1†). $PtNP_{20}$, $PtNP_{30}$, $PtNP_{75}$, and $PtNP_{95}$ exhibited monomodal PSDs, whereas $PtNP_{50}$ exhibited a bimodal PSD (Fig. 1a). The mean core diameters of $PtNP_{20}$, $PtNP_{30}$, $PtNP_{50}$, $PtNP_{75}$, and $PtNP_{95}$ measured by TEM are 9.2 ± 1.2, 10.9 ± 0.8, 18.5 ± 5, 44.5 ± 5, and 72.5 ± 3.9 nm, respectively (Table S7†). sp-ICP-MS analysis show that all PVP-PtNPs exhibited monomodal PSDs, with mean core diameters for $PtNP_{20}$–$PtNP_{95}$ of 26.4 ± 11.6, 30.2 ± 12.9, 34.3 ± 10.1, 44.1 ± 7.7, and 76.7 ± 9.7 nm, respectively (Fig. 1b, Table S8†). The mean core diameters for PVP-$PtNP_{75}$ and PVP-$PtNP_{95}$ measured by sp-ICP-MS are in good aggrement with those measured by TEM (Table S7†). However, the mean core diameters of PVP-$PtNP_{20}$, PVP-$PtNP_{30}$, and PVP-$PtNP_{50}$ measured by sp-ICP-MS were larger than those measured by TEM (Table S7†). These size differences can be attributed to the greater size detection limit of sp-ICP-MS for PVP-PtNP (*e.g.*, 18 nm[58]) compared to TEM (*e.g.*, typically <1 nm, depending on the TEM spectrum and operating condition[59]). The PSDs of PVP-$PtNP_{20}$, PVP-$PtNP_{30}$, and PVP-$PtNP_{50}$ obtained by sp-ICP-MS are monomodal but represent curtailed log-normal size distribution, resulting in greater mean core sizes compared to those measured by TEM.

The number concentration of PVP-$PtNP_{20}$, PVP-$PtNP_{30}$, and PVP-$PtNP_{50}$ in UPW measured by sp-ICP-MS represents a small fraction (*e.g.*, 0.3, 1.2, and 33.1%, respectively) of the theoretical particle number concentration (Table S8†). In contrast, the measured number concentrations of PVP-$PtNP_{75}$ and PVP-$PtNP_{95}$ in UPW were in good agreement with the theoretical number concentration (Table S8†). This is attributed to the size detection limit of sp-ICP-MS.[58] The number PSD measured by TEM illustrates that all NPs in PVP-$PtNP_{20}$, and PVP-$PtNP_{30}$ and 54% of NPs in PVP-$PtNP_{50}$ are below the sp-ICP-MS size detection limit, whereas all particles in PVP-$PtNP_{75}$ and PVP-$PtNP_{95}$ are larger than the sp-ICP-MS size detection limit for PtNPs (Fig. 1b).

The zeta potential of the synthesized PVP-PtNPs decreased from −16.9 ± 3.5 to −27.2 ± 1.7 with the increase in particle size (Table S7†), which might be attributed to the partial coating of PtNPs. Typically, NPs fully coated with PVP molecules exhibit low zeta potential of approximately −10 mV.[60,61] Higher zeta potential of PVP-coated NPs has been reported elsewhere and was attributed to the partial surface coating of NPs by PVP molecules.[62–64] For instance, the magnitude of the zeta potential of PVP-partially coated AgNPs increased with a decrease in the number of PVP molecules per AgNP unit surface area.[2]

Size-dependent aggregation of PVP-PtNPs

The number PSDs of PVP-$PtNP_{20}$–PVP-$PtNP_{75}$ exhibited a modest shift towards larger sizes immediately after mixing with MHW (0 h) relative to the corresponding PSDs of PVP-$PtNP_{20}$–PVP-$PtNP_{75}$ measured in UPW (Fig. 2a–d). After 24 h in MHW, the PSDs of PVP-$PtNP_{20}$–PVP-$PtNP_{75}$ shifted further towards larger sizes, which indicates PVP-PtNP aggregation in MHW. The aggregation of PVP-PtNPs in MHW relative to UPW can be attributed to the higher ionic strength of the MHW which screens the PVP-PtNP surface charge. The magnitude of the zeta potential of each PVP-PtNP suspension (1 mg L^{-1}) decreased in MHW at 0 h and further decreased at

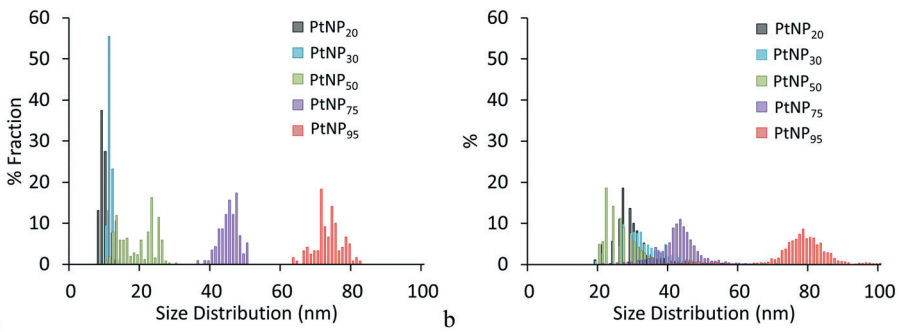

Fig. 1 Number particle size distribution of polyvinylpyrrolidone-coated platinum nanoparticles of five different nominal sizes ranging from 20 to 95 nm (denoted as $PtNP_{20}$–$PtNP_{95}$) measured by (a) transmission electron microscope (TEM), and (b) single particle-inductively coupled plasma-mass spectrometer (sp-ICP-MS). Size detection limit of PtNPs in sp-ICP-MS is 18 nm.

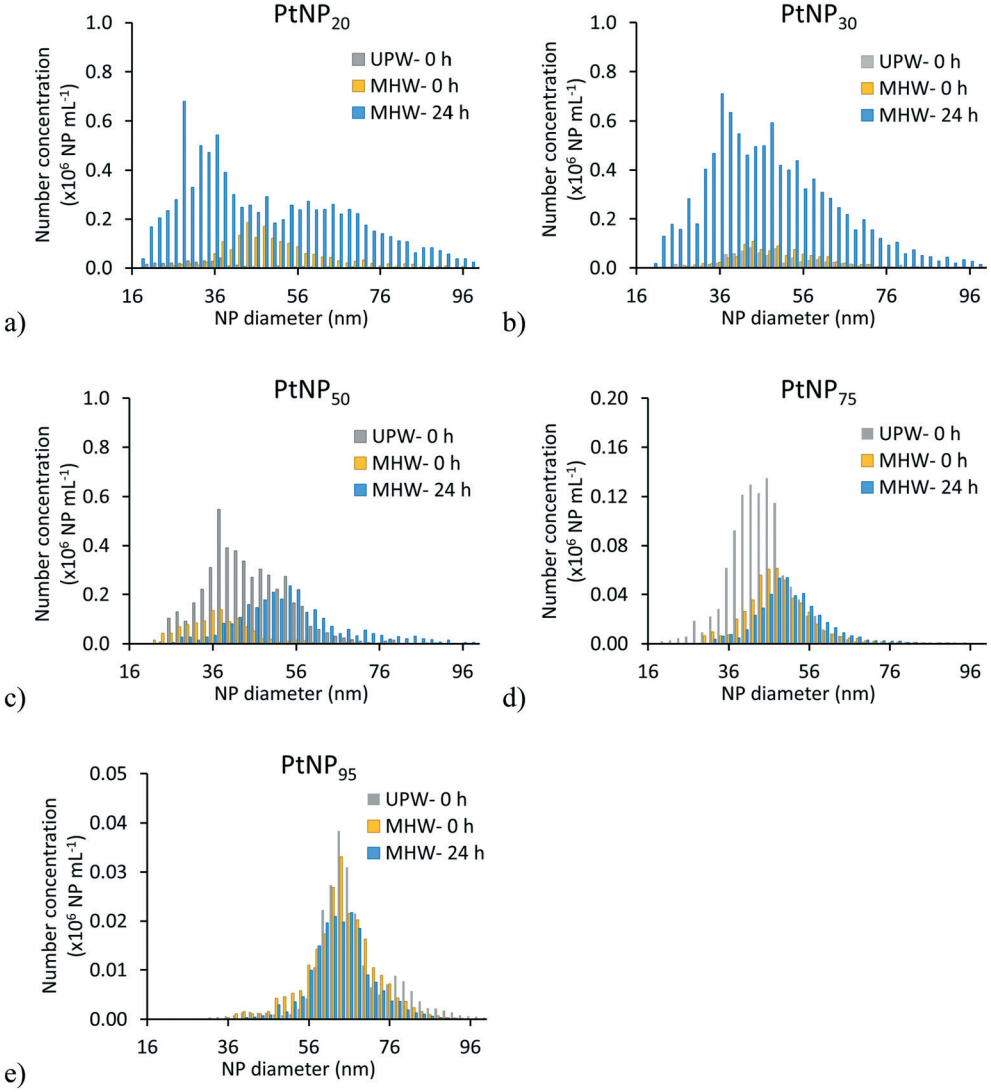

Fig. 2 Number particle size distribution (PSDs) measured by sp-ICP-MS of 1 μg L^{-1} PVP-PtNPs in ultrapure water (UPW) at 0 and 24 h after mixing with moderately hard water (MHW) of: (a) $PtNP_{20}$, (b) $PtNP_{30}$, (c) $PtNP_{50}$, (d) $PtNP_{75}$, and (e) $PtNP_{95}$.

24 h relative to the corresponding zeta potential measured in UPW (Table S9†). The number PSD of PVP-$PtNP_{95}$ did not change in MHW relative to that measured in UPW (Fig. 2e), indicating that PVP-$PtNP_{95}$ are stable in MHW.

The number concentrations of PVP-$PtNP_{20}$ and PVP-$PtNP_{30}$ increased immediately after mixing with MHW relative to those measured in UPW and increased further after 24 h (Table S8†). This observation is counterintuitive, as one would expect NP number to decrease with NP aggregation. However, due to aggregation, PVP-PtNP aggregate size became larger than the size detection limit of sp-ICP-MS for PtNPs (*i.e.*, 18 nm). Thus, NP aggregation increased the detectable PtNPs by sp-ICP-MS and increased the measured PVP-PtNP number concentration (Table S8† and Fig. 2a and b). This is corroborated by the increase in mass concentration of PVP-$PtNP_{20}$ and PVP-$PtNP_{30}$ measured by sp-ICP-MS in MHW relative to those measured in UPW (Table S10†).

The number concentration of PVP-$PtNP_{50}$ and PVP-PtNP75 decreased immediately after mixing with MHW relative to the number concentration in UPW and decreased further after 24 h of mixing with MHW (Table S8†), which can be attributed to particle aggregation. Aggregation of PVP-$PtNP_{50}$ should increase the number particle concentration, as observed for PVP-$PtNP_{20}$ and PVP-$PtNP_{30}$. However, only 33% of NPs in PVP-$PtNP_{50}$ were smaller than the sp-ICP-MS size detection limit. Thus, aggregation of PVP-$PtNP_{50}$ increases the size of undetectable particles to become detectable and thus increase the number particle concentration, but aggregation also reduces the number of NPs larger than the sp-ICP-MS detection limit. Thus, the measured number concentration is influenced by these two counteracting processes. All NPs in PVP-$PtNP_{75}$ were larger than the size detection limit of sp-ICP-MS and thus the number concentration of PVP-$PtNP_{75}$ in MHW decreased relative to that in UPW due to particle aggregation. The number concentrations of PVP-$PtNP_{95}$ in UPW and in MHW at t = 0

were not statistically different ($p < 0.05$) (Table S8†). The number concentration of PVP-PtNP$_{95}$ in MHW decreased (*e.g.*, 35% reduction, Table S8†) after 24 h in MHW, but the number PSD of PVP-PtNP$_{95}$ did not change after 24 h in MHW. This might be due to the aggregation of some PVP-PtNPs without a significant shift in the number PSD, or to sedimentation of some PVP-PtNPs, or to both processes. Nevertheless, the decrease in PVP-PtNP$_{75}$ and PVP-PtNP$_{95}$ mass concentration suggest a loss of some PVP-PtNPs, most likely due to PVP-PtNP sedimentation. Sedimentation of PVP-PtNP$_{75}$ and PVP-PtNP$_{95}$ was observed in the stock suspensions within 24–48 h, mainly because of the high density of PtNPs (21.45 g cm^{-3}). Similar gravitational sedimentation of 65 and 87.5 nm AuNPs (density = 19.32 g cm^{-3}) in UPW under static condition was observed after 48 h.[65]

The number PSD of PVP-PtNP$_{20}$ and PVP-PtNP$_{30}$ 24 h after mixing with MHW (Fig. 2a and b) exhibited broader size distributions compared to PVP-PtNP$_{50}$, PVP-PtNP$_{75}$, and PVP-PtNP$_{95}$ (Fig. 2c–e). This observation indicates that smaller PVP-PtNPs are more prone to aggregation and form larger aggregates compared those formed by the aggregation of larger PVP-PtNPs. This is consistent with previous studies demonstrating an increased aggregation of smaller hematite NPs,[3] TiO_2 NPs,[4,66] and cit-PtNPs under the same experimental conditions relative to their larger counterpart.[7] NP aggregation occurs because of NP collision and attachment. Collision increases with the increase in NP number concentration, whereas attachment increases with the decrease in NP zeta potential. At the same mass concentration, NP number concentration increases with the

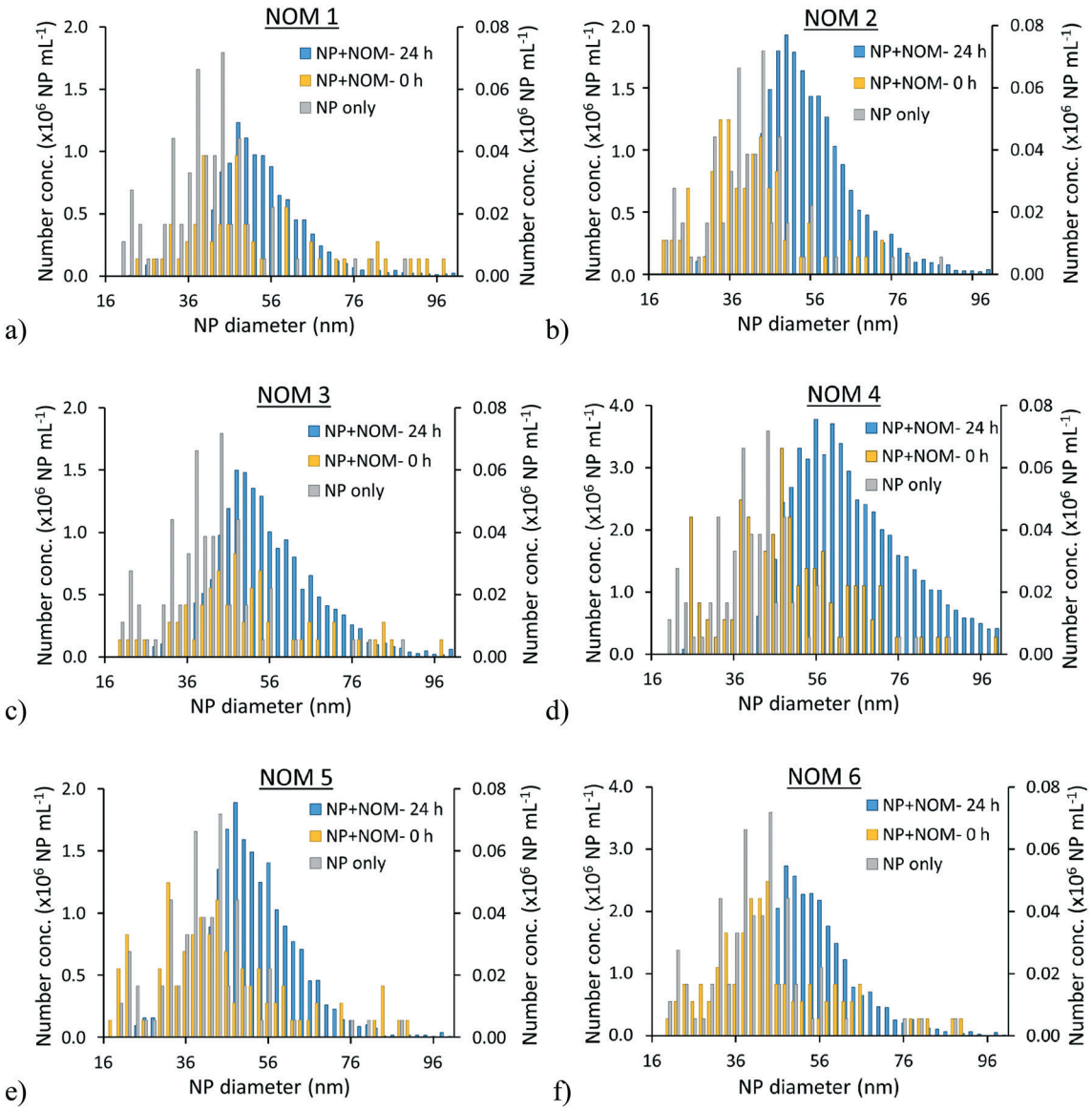

Fig. 3 Particle size distribution (PSD) measured by sp-ICP-MS of 1 μg L^{-1} PtNP$_{20}$ at 0 and 24 hours after mixing with MHW in the presence of 1 mg L^{-1} (a) NOM 1, (b) NOM 2, (c) NOM 3, (d) NOM 4, (e) NOM 5, and (f) NOM 6. The number concentration of PtNPs only and PtNPs + NOM- at 0 h are presented on the secondary *Y*-axis.

decrease in NP size. The magnitude of zeta potential decreases with decreasing NP size (Table S9†). Thus, both factors (zeta potential, NP number concentration) contribute to the increased aggregation with decreasing PVP-PtNP sizes. However, positive correlation[2,5] and insignificant correlation[6] between primary particle size and aggregation were also reported in literature. The detection of small particles in PVP-$PtNP_{20}$, PVP-$PtNP_{30}$, and PVP-$PtNP_{50}$ suspensions (Fig. 2a–c) after 24 in MHW that were not detected in the corresponding suspensions in UPW is attributed to the aggregation of PVP-PtNPs that are smaller than the sp-ICP-MS size detection limit in MHW.

NOM-dependent aggregation of PVP-PtNPs

The PSDs of PVP-$PtNP_{20}$ (1 μg L^{-1}) in MHW in the presence of NOM (1 mg L^{-1}) samples at time 0 h were not statistically different (Kolmogorov–Smirnov test; *p*- value >0.065) than the PSD of PVP-$PtNP_{20}$ measured in MHW (without NOM) at time 0 h (Fig. 3), suggesting a lack of immediate aggregation of PVP-$PtNP_{20}$ in MHW in the presence of NOM. After 24 h, the PSDs of PVP-$PtNP_{20}$ in the presence of NOM samples shifted toward larger sizes relative to the measured PSD at time 0 h, indicating aggregation of PVP-$PtNP_{20}$ in MHW in the presence of all NOM samples after 24 hours. Whereas the PSD of PVP-$PtNP_{20}$ after 24 hours mixing in MHW displayed a bimodal distribution (Fig. 2a), the PSDs of PVP-$PtNP_{20}$ in the presence of the different NOMs exhibited monomodal distributions (Fig. 3). The PSDs of PVP-$PtNP_{20}$ in presence of NOM 1, 2, 3, 5, and 6 after 24 h in MHW were not statically different (Kolmogorov–Smirnov test; $p > 0.4$) relative to the PSD of PVP-$PtNP_{20}$ after 24 h in MHW without NOM. However, the PSDs of PVP-$PtNP_{20}$ in the presence of NOM 4 after 24 h in MHW was statically different (larger, Kolmogorov–Smirnov test; $p < 0.05$) relative to the PSD of PVP-$PtNP_{20}$ after 24 h in MHW without NOM. Similarly, the mean number diameters of PVP-$PtNP_{20}$ in the presence of NOM 1, 2, 3, 5 and 6 (Table S11†), were not significantly different (*t*-test; $p > 0.05$) relative to the mean diameter of PVP-$PtNP_{20}$ after 24 h in MHW without NOM. In contrast, the mean diameter of PVP-$PtNP_{20}$ in the presence of NOM 4 (Pacific Ocean HPOA) was larger than the mean diameter of PVP-$PtNP_{20}$ in MHW without NOM and in MHW in the presence of all other NOM samples (*t*-test; $p < 0.05$). These results suggest that NOM differently impacted PVP-$PtNP_{20}$ aggregation and stability.

To evaluate PVP-PtNPs aggregation in the absence and presence of NOM, the number and mass concentrations of PVP-PtNPs measured by sp-ICP-MS were compared to the theoretical number and mass concentrations, respectively. The number concentration of PVP-$PtNP_{20}$ after mixing with MHW in the presence of NOM samples increased from <1% at 0 h to 11–52% at 24 h of the theoretical PVP-$PtNP_{20}$ number concentration, respectively (Table S11†), confirming the aggregation of PVP-$PtNP_{20}$ in MHW in the presence and/or absence of NOM. In contrast, PVP-$PtNP_{20}$ in UPW did not aggregate during 24 h exposure and the number concentration of PVP-$PtNP_{20}$ remained constant and represented only 0.7% of the theoretical PVP-$PtNP_{20}$ concentration. The mass concentration of PVP-$PtNP_{20}$ in the presence and absence NOM samples also followed the same trend. The mass concentration of PVP-$PtNP_{20}$ after mixing with MHW in the presence of NOM samples increased from <4% 0 h to 19 to 98% at 24 of the theoretical PVP-$PtNP_{20}$ mass concentration (Table S12†).

The number concentration of PVP-$PtNP_{20}$ in presence of NOM 4 was significantly higher than the number concentration of PVP-$PtNP_{20}$ in the absence of NOM (Fig. 4a; $p < 0.05$), whereas the number concentration of PVP-$PtNP_{20}$ in the presence of NOM 1, 2, 3, 5, and 6 were not significantly different compared to the number concentration of PVP-$PtNP_{20}$ in the absence of NOM (Fig. 4a; ANOVA with Tuckey's multiple comparison test; $\alpha = 0.05$). The mass concentration of PVP-$PtNP_{20}$ in the presence of NOM 4 was larger than the mass concentration of PVP-$PtNP_{20}$ in the absence of NOM and in the presence all other NOM samples. However, the mass concentration of PVP-$PtNP_{20}$ in the presence of NOM 1, 2, 3, 5, and 6 were not significantly different relative to the mass concentration of PVP-$PtNP_{20}$ in the absence of NOM (Fig. 4b; ANOVA with Tuckey's multiple comparison; $\alpha = 0.05$). The mass concentration of PVP-$PtNP_{20}$ in the presence of NOM 1 was lower than the mass concentration of PVP-$PtNP_{20}$ in the presence of NOM 2 (ANOVA with Tuckey's multiple comparison test; $\alpha = 0.05$), whereas the mass concentration of PVP-$PtNP_{20}$ in the presence of NOM 2, 3, 5 and 6 were not significantly different among themselves. These results indicate that NOM 4 influenced PVP-$PtNP_{20}$ aggregation differently than all other NOM samples. Below we discuss how the molecular composition and properties of the NOM samples help explain differences in how NOM affects PVP-$PtNP_{20}$ aggregation.

We interpret the increased aggregation of PVP-$PtNP_{20}$ in the presence of NOM to be a result of inter-particle bridging of NOM-coated PVP-PtNPs due to complex formation between humic acid macromolecules and divalent counterions (*e.g.*, Ca^{2+} and Mg^{2+}). This is agreement with the bridging of PVP-AuNPs in the presence of NOM and high concentrations of Ca^{2+} and Mg^{2+}.[67] The concentrations of monovalent counterions in MHW (*e.g.*, 1.14 mM Na^+ and 0.05 mM K^+, Table S3†) are lower than that (*e.g.*, ≥50 mM Na^+) required to initiate PVP-$PtNP_{20}$ aggregation.[7] However, the concentrations of divalent counterions in MHW (*e.g.*, 0.45 mM Ca^{2+} and 0.5 mM Mg^{2+}, Table S6†) are in close proximity to the critical coagulation concentration (*e.g.*, 1.1 Ca^{2+}) for PVP-$PtNP_{20}$ and thus can result in a significant aggregation of PVP-$PtNP_{20}$.[7] However, this bridging phenomenon may depend on the type, composition and structure of the NOM, which has not been investigated previously.

The PSD of PVP-$PtNP_{95}$ in MHW in the presence of NOM samples at 0 and 24 h (Fig. 5) were not statistically different from those measured in MHW at time 0 h or 24 h (Fig. 2e). This observation indicates that all NOM samples did not have significant impact on the colloidal stability of PVP-$PtNP_{95}$. The number concentration of PVP–PVP-$PtNP_{95}$ decreased

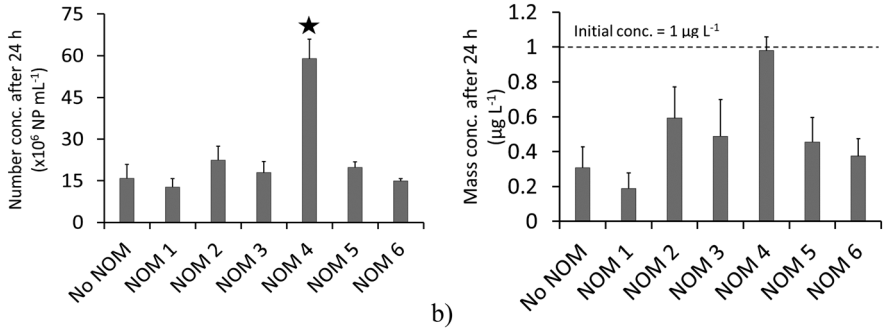

Fig. 4 (a) Number and (b) mass concentration of 1 μg L^{-1} $PtNP_{20}$ measured by sp-ICP-MS after 24 h of mixing with MHW in the absence and presence of 1 mg L^{-1} NOM. * represents a significant increase in measured $PtNP_{20}$ number concentration in the presence of NOM compared to that measured in the absence of NOM.

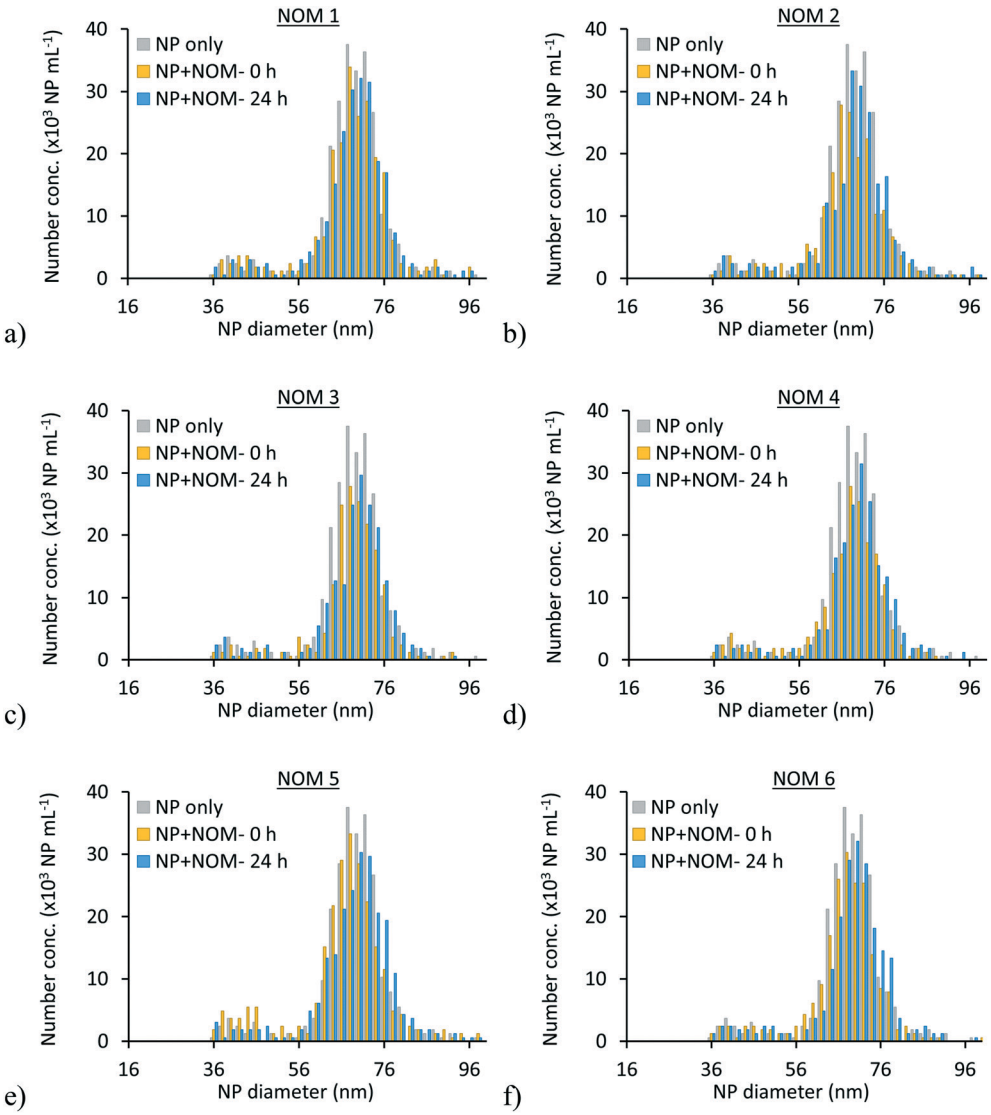

Fig. 5 Particle size distribution of $PtNP_{95}$ measured by sp-ICP-MS of 1 μg L^{-1} $PtNP_{95}$ at 0 h and 24 h after mixing with MHW in the presence of 1 mg L^{-1} (a) NOM 1, (b) NOM 2, (c) NOM 3, (d) NOM 4, (e) NOM 5, and (f) NOM 6.

slightly in MHW relative to that measured in UPW at 24 h (Table S13†), indicating slight particle aggregation and/or sedimentation. The mass concentration of PVP-$PtNP_{95}$ decreased slightly in MHW relative to that measured in UPW at 24 h (Table S14†) indicating modest particle aggregation and/or sedimentation of PVP-PtNPs during this period. The

number and mass concentrations of PVP-PtNP$_{95}$ in MHW increased slightly in the presence of all NOM samples relative to treatments without NOM, suggesting that the presence of NOM enhanced the stability of PVP-PtNP$_{95}$.

Taken together, these results suggest that the effect of NOM on PVP-PtNP aggregation is size-dependent. The stability of smaller PVP-PtNPs appeared more influenced by NOM than that of the larger PVP-PtNPs, which might be attributed to the size-dependent NOM-corona composition/properties. For instance, Pettibone *et al.* (2008) demonstrated differences in adsorption sites or the distribution of adsorption sites for oxalic acid on the surfaces of 5 nm and 32 nm TiO_2-NPs, which was attributed to greater abundance of lower energy binding sites, associated with edge and corner sites, available for adsorption of oxalic acids on the surfaces of 5 nm TiO_2-NPs compared to that on the surfaces of 32 nm TiO_2-NPs.[66] Differences in adsorption sites on NP surfaces can be even more important for the adsoption of NOM on NP surfaces due to polydiversity of NOM formulas. Zhang *et al.* (1999) reported increased adsorption of organic acids with decreasing (*e.g.*, 6–16 nm) TiO_2 NP sizes.[68] Smaller particles with increased molar free energy are more prone to adsorb molecules or ions per unit area onto their surfaces in order to decrease the total free energy and become more stable.[68] Chowdhury *et al.* (2013) reported that NOM affect the morphology of TiO_2 NP aggregates, where small NPs (*e.g.*, 6 nm) form more compact aggregates than larger NPs in the presence of NOM (*e.g.*, 13 nm and 23), suggesting that interactions of NOM with smaller NPs are more significant than those with larger ones.[77] At a fixed mass concentration, larger NPs display a smaller total surface area (Table S8†). Therefore, at a fixed NOM concentration, higher number of NOM molcules are available for interaction with larger NP surfaces per unit surface area. This may enhance the stability of larger particles compared to that of smaller NPs in the presence of NOMs.

Correlating PVP-PtNP$_{20}$ aggregation to NOM molecular properties

The NOM samples used in this study represents a diverse array of NOM compositional differences relevant to all aquatic systems. Differences in NOM composition among samples may explain the variation in the observed particle aggregation. To identify the NOM properties with the greatest influence on NP aggregation, we performed Pearson's correlation analysis between mass of aggregated PVP-PtNP$_{20}$ and specific NOM properties. PVP-PtNP$_{95}$ were not included in these correlation analysis as they did not exhibit any appreciable aggregation in the presence or absence of NOM.

Bulk and molecular-level properties of NOM samples provided robust prediction of the aggregation of PVP-PtNP$_{20}$. Negative correlations of statistical significance were observed between the mass of aggregated PVP-PtNP$_{20}$ and NOM MW (r = −0.979, p = 0.004), SUVA$_{254}$ (r = −0.763, p = 0.078), O/C ratio (r = −0.841, p = 0.036), relative abundance of condensed hydrocarbons (ConHC, r = −0.766, p = 0.076), and relative abundance of tannin molecules (r = −0.898, p = 0.015). Positive correlations of statistical significance were observed between the mass of aggregated PVP-PtNP$_{20}$ and NOM H/C (r = 0.73, p = 0.1) and relative abundancies of lignin/CRAM (r = 0.798, p = 0.058) (Tables 1 and S4–S6 and Fig. 6 and S3†).

Correlations between PVP-PtNP$_{20}$ aggregation and NOM properties are interpreted to reflect differences in molecular hydrophobicity and charge density. Aggregation of PVP-PtNP$_{20}$ was limited in the presence of NOM that was more hydrophobic, as measured by SUVA$_{254}$ (Fig. 6b), abundance of condensed hydrocarbon (Fig. 6c), and H/C, a measure of hydrogen saturation (Fig. S3e†). NOM samples with higher SUVA$_{254}$ and relative abundance of ConHC are expected to result in higher sorption of these molecules on NP surfaces and thus increasing the NP hydrophobicity, and thus may enhance repulsive forces between NPs. NOM samples with higher average MW, which also co-varies with aromaticity,[69] would presumably lead to thicker adsorbed layers of NOM on NP surfaces, resulting in increased steric stabilization.[70–72] Aggregation of PVP-PtNP$_{20}$ was also influenced by the charge density of the NOM, as measured principally by the O/C (Fig. S3d†). NOM sample with higher O/C, and thus higher charge density, demonstrated negative correlation with the observed aggregation (Table 1). In contrast, NOM samples with lower charge density parameters (*i.e.*, low O/C) showed positive correlation with the aggregated mass (Table 1). Higher oxygen content and O/C ratio indicates a higher content of functional groups such as carboxylic and carbonyl groups.[26] The higher content of these functional groups is likely to enhance NP surface charge, which increases the electrostatic repulsive forces between NOM-coated PVP-PtNPs, and thus enhances NP stability.[26] In summary, aggregation of PVP-PtNPs is interpreted to be a function of both the NOM hydrophobicity and charge density, and the selective sorption of NOM molecules to NP surfaces that control NP stability.[73–78] Similar observations have been made for ZnS NPs[26] and cit-AuNPs.[24] Thus, larger MW, higher SUVA$_{254}$, and relative abundance of ConHC in NOM samples enhance NP$_{20}$ stability.[24,26]

NOM molecules with high O/C (*i.e.*, tannin) demonstrated significant negative correlation, whereas those with lower O/C (*i.e.*, lignin/CRAM, conHC *etc.*) demonstrated significant positive correlation with the mass of aggregated PVP-PtNP$_{20}$, in good agreement with the correlations observed with O/C ratios as discussed above. Lignin/CRAM- and tannin- like compounds contain the same types of surface functional groups (hydroxyl, carbonyl groups and phenol groups). However, tannins are high molecular weight polycyclic aromatic compounds with high O/C ratio and charge density than CRAM molecules, which is likely to enhance the NP surface charge, and thus, result in higher NP stability. Additionally, the hydrophobic nature and polymer structure of tannins might be responsible for increased NP stability and decreased aggregation.[79] Lignin/CRAM are high molecular polyphenolic compounds.[79] These poly-phenol compounds have particular importance as they promote aggregation by forming strong non-covalent bonds.[80] Lignin/

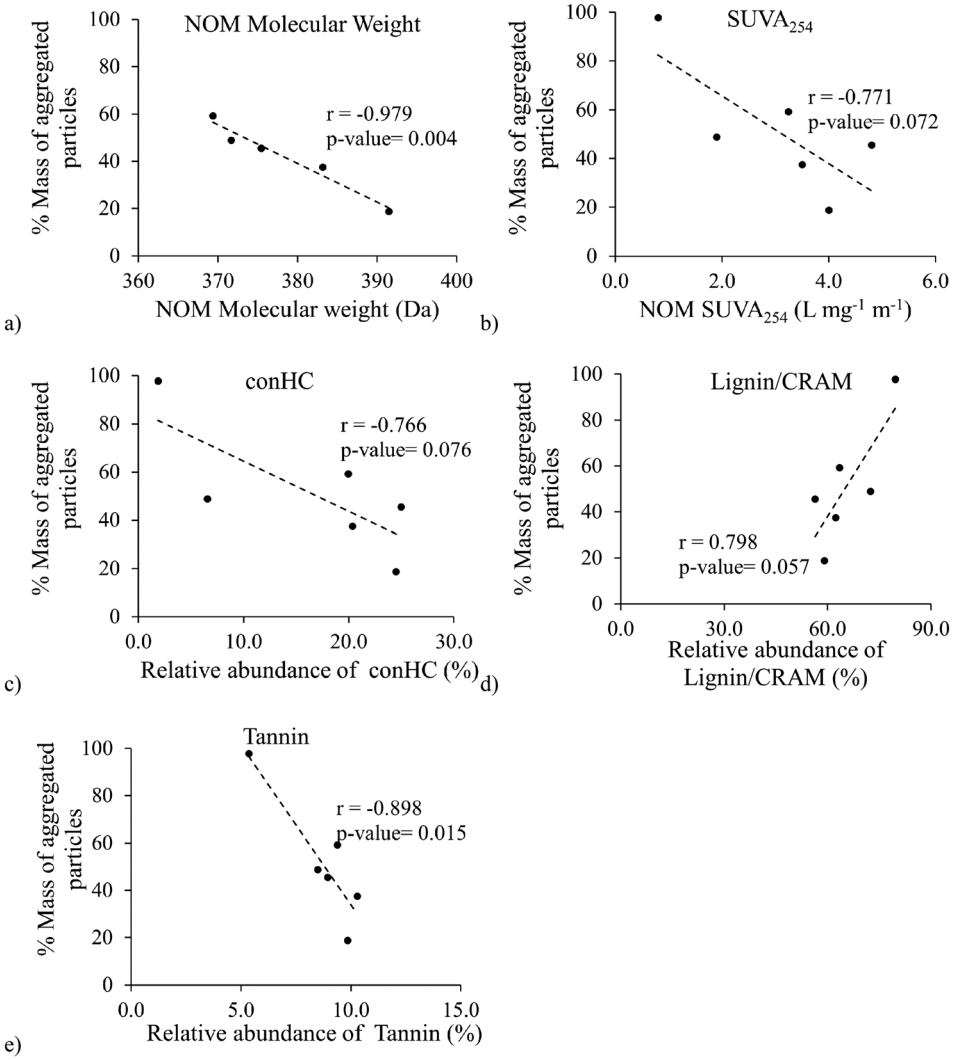

Fig. 6 Correlation between % of $PtNP_{20}$ mass undergoing aggregation in the presence of the different NOM isolates and NOM properties: (a) molecular weight, (b) specific UV absorbance at 254 nm ($SUVA_{254}$), (c) condensed hydrocarbon (ConHC), (d) lignin/carboxyl-rich alicyclic molecules (CRAM), and (e) tannin. The Pearson's correlation coefficient (*r*) and *p*-values of linear regressions are presented for each plot.

CRAM have hydrophilic regions such as hydroxyls (–OH), carboxylic (–COOH) and small alkyl chains *i.e.*, methane groups ($–CH_3$). These functional groups and the hydrophobic regions of lignin/CRAM (*e.g.*, resinol, C–H groups) enable it to bind with nanoparticle surfaces through polar, covalent, and hydrogen bonding as well as Van der Waals forces. These humidified and highly decomposed materials, which are more stable, aid in the formation of microaggregates.[81] For instance, lignin has been shown to promote macroaggregation in soil and to increase aggregate stability.[81–83]

Conclusions

This study demonstrated that aggregation of PVP-PtNPs depend on several factors, including NP size and NOM characteristics. At the same mass concentration, PVP-PtNP aggregate size increased with the decrease in NP primary size due to the increased NP number concentration and therefore collision frequency. NOM samples of different compositions and properties did not alter the aggregation behavior of PVP-$PtNP_{95}$ in MHW. However, the same NOM samples generally increased the aggregation of PVP–PVP-$PtNP_{20}$ in MHW to different extents, likely *via* bridging mechanism(s) in the presence of divalent counterions in MHW. The mass of aggregated PVP-$PtNP_{20}$ decreased with the increase in NOM elemental ratio of O/C, molecular weight, $SUVA_{254}$, and relative abundance of condensed hydrocarbons and tannin. The mass of the aggregated PVP-$PtNP_{20}$ increased with the increase in NOM elemental ratio of H/C and the relative abundance of lignin/CRAM formulas. Therefore, the molecular composition and properties, and thus sources, of NOM may determine to a great extent PVP-PtNP colloidal stability in aquatic environments.

Future studies are needed to unravel the complex and subtle impacts of NOM composition and properties on NP stability. Specifically, information is needed on NP stability under

various conditions of NOM concentration (*e.g.*, 1 to 30 mg C per L), NP concentration (*e.g.*, μg L^{-1} to mg L^{-1}) and properties (*e.g.*, size, shape, and surface coating), water physicochemical properties (*e.g.*, pH, ionic strength and composition), presence of suspended particulate matter, water dynamics (*e.g.*, static *vs.* stirring, or water turbulence), and aging time (*e.g.*, weeks and months). Future efforts on the stability of PtNPs and that of other NPs is needed to develop quantitative structure activity relationships between NOM molecular properties and the environmental behaviors of NPs.

Conflicts of interest

There are no conflicts to declare.

Acknowledgements

This work was supported by US National Science Foundation NSF-EPSCoR Fellowship (1738340) to Dr. Mohammed Baalousha. A portion of this research was performed using EMSL, a DOE Office of Science User Facility sponsored by the Office of Biological and Environmental Research. Any use of trade, firm, or product names is for descriptive purposes only and does not imply endorsement by the U.S. Government.

References

1 M. Baalousha, Effect of nanomaterial and media physicochemical properties on nanomaterial aggregation kinetics, *NanoImpact*, 2017, **6**, 55–68.
2 K. Afshinnia, M. Sikder, B. Cai and M. Baalousha, Effect of nanomaterial and media physicochemical properties on Ag NM aggregation kinetics, *J. Colloid Interface Sci.*, 2017, **487**, 192–200.
3 Y. T. He, J. Wan and T. Tokunaga, Kinetic stability of hematite nanoparticles: the effect of particle sizes, *J. Nanopart. Res.*, 2008, **10**(2), 321–332.
4 D. Zhou, Z. Ji, X. Jiang, D. R. Dunphy, J. Brinker and A. A. Keller, Influence of Material Properties on TiO2 Nanoparticle Agglomeration, *PLoS One*, 2013, **8**(11), e81239.
5 M. J. Mulvihill, S. E. Habas, I. Jen-La Plante, J. Wan and T. Mokari, Influence of Size, Shape, and Surface Coating on the Stability of Aqueous Suspensions of CdSe Nanoparticles, *Chem. Mater.*, 2010, **22**(18), 5251–5257.
6 J. Liu, S. Legros, G. Ma, J. G. C. Veinot, F. von der Kammer and T. Hofmann, Influence of surface functionalization and particle size on the aggregation kinetics of engineered nanoparticles, *Chemosphere*, 2012, **87**(8), 918–924.
7 M. Sikder, J. Wang, G. T. Chandler, D. Berti and M. Baalousha, Synthesis, characterization, and environmental behaviors of monodispersed platinum nanoparticles, *J. Colloid Interface Sci.*, 2019, **540**, 330–341.
8 J. A. Leenheer and J. P. Croue, Characterizing aquatic dissolved organic matter, *Environ. Sci. Technol.*, 2003, **37**(1), 18a–26a.
9 A. Nebbioso and A. Piccolo, Molecular characterization of dissolved organic matter(DOM): a critical review, *Anal. Bioanal. Chem.*, 2013, **405**(1), 109–124.
10 R. G. M. Spencer, K. D. Butler and G. R. Aiken, Dissolved organic carbon and chromophoric dissolved organic matter properties of rivers in the USA, *J. Geophys. Res.: Biogeosci.*, 2012, **117**, G03001, DOI: 10.1029/2011JG001928.
11 A. A. Keller, H. Wang, D. Zhou, H. S. Lenihan, G. Cherr, B. J. Cardinale, R. Miller and Z. Ji, Stability and Aggregation of Metal Oxide Nanoparticles in Natural Aqueous Matrices, *Environ. Sci. Technol.*, 2010, **44**(6), 1962–1967.
12 A. R. Petosa, D. P. Jaisi, I. R. Quevedo, M. Elimelech and N. Tufenkji, Aggregation and Deposition of Engineered Nanomaterials in Aquatic Environments: Role of Physicochemical Interactions, *Environ. Sci. Technol.*, 2010, **44**(17), 6532–6549.
13 B. Gu, J. Schmitt, Z. Chen, L. Liang and J. F. McCarthy, Adsorption and desorption of different organic matter fractions on iron oxide, *Geochim. Cosmochim. Acta*, 1995, **59**(2), 219–229.
14 C. T. Gibson, I. J. Turner, C. J. Roberts and J. R. Lead, Quantifying the Dimensions of Nanoscale Organic Surface Layers in Natural Waters, *Environ. Sci. Technol.*, 2007, **41**(4), 1339–1344.
15 I. Lynch, K. A. Dawson, J. R. Lead and E. Valsami-Jones, Macromolecular coronas and their importance in nanotoxicology and nanoecotoxicology, in *Nanoscience and the Environment*, ed. J. R. Lead and E. Valsami-Jones, *Frontiers of Nanoscience*, Elsevier, 2014, pp. 127–156.
16 B. L. T. Lau, W. C. Hockaday, K. Ikuma, O. Furman and A. W. Decho, A preliminary assessment of the interactions between the capping agents of silver nanoparticles and environmental organics, *Colloids Surf., A*, 2013, **435**, 22–27.
17 S. Diegoli, A. L. Manciulea, S. Begum, I. P. Jones, J. R. Lead and J. A. Preece, Interaction between manufactured gold nanoparticles and naturally occurring organic macromolecules, *Sci. Total Environ.*, 2008, **402**(1), 51–61.
18 A. P. Gondikas, A. Morris, B. C. Reinsch, S. M. Marinakos, G. V. Lowry and H. Hsu-Kim, Cysteine-Induced Modifications of Zero-valent Silver Nanomaterials: Implications for Particle Surface Chemistry, Aggregation, Dissolution, and Silver Speciation, *Environ. Sci. Technol.*, 2012, **46**(13), 7037–7045.
19 F. Mohd Omar, H. Abdul Aziz and S. Stoll, Aggregation and disaggregation of ZnO nanoparticles: Influence of pH and adsorption of Suwannee River humic acid, *Sci. Total Environ.*, 2014, **468-469**, 195–201.
20 S. Ghosh, W. Jiang, J. D. McClements and B. Xing, Colloidal Stability of Magnetic Iron Oxide Nanoparticles: Influence of Natural Organic Matter and Synthetic Polyelectrolytes, *Langmuir*, 2011, **27**(13), 8036–8043.
21 F. Loosli, P. Le Coustumer and S. Stoll, TiO2 nanoparticles aggregation and disaggregation in presence of alginate and Suwannee River humic acids. pH and concentration effects on nanoparticle stability, *Water Res.*, 2013, **47**(16), 6052–6063.
22 S. M. Louie, E. R. Spielman-Sun, M. J. Small, R. D. Tilton and G. V. Lowry, Correlation of the Physicochemical Properties of Natural Organic Matter Samples from Different Sources to Their Effects on Gold Nanoparticle Aggregation in Monovalent Electrolyte, *Environ. Sci. Technol.*, 2015, **49**(4), 2188–2198.

23 S. M. Louie, R. D. Tilton and G. V. Lowry, Effects of Molecular Weight Distribution and Chemical Properties of Natural Organic Matter on Gold Nanoparticle Aggregation, *Environ. Sci. Technol.*, 2013, **47**(9), 4245–4254.
24 J. A. Nason, S. A. McDowell and T. W. Callahan, Effects of natural organic matter type and concentration on the aggregation of citrate-stabilized gold nanoparticles, *J. Environ. Monit.*, 2012, **14**(7), 1885–1892.
25 M. H. Shen, Y. G. Yin, A. Booth and J. F. Liu, Effects of molecular weight-dependent physicochemical heterogeneity of natural organic matter on the aggregation of fullerene nanoparticles in mono- and di-valent electrolyte solutions, *Water Res.*, 2015, **71**, 11–20.
26 A. Deonarine, B. L. T. Lau, G. R. Aiken, J. N. Ryan and H. Hsu-Kim, Effects of Humic Substances on Precipitation and Aggregation of Zinc Sulfide Nanoparticles, *Environ. Sci. Technol.*, 2011, **45**(8), 3217–3223.
27 J. D'Andrilli, T. Dittmar, B. P. Koch, J. M. Purcell, A. G. Marshall and W. T. Cooper, Comprehensive characterization of marine dissolved organic matter by Fourier transform ion cyclotron resonance mass spectrometry with electrospray and atmospheric pressure photoionization, *Rapid Commun. Mass Spectrom.*, 2010, **24**(5), 643–650.
28 M. Sikder, J. Wang, G. Thomas Chandler, D. Berti and M. Baalousha, Synthesis, Characterization, and Environmental Behaviors of Monodispersed Platinum Nanoparticles, *J. Colloid Interface Sci.*, 2019, 330–341.
29 V. Filipe, A. Hawe and W. Jiskoot, Critical Evaluation of Nanoparticle Tracking Analysis(NTA) by NanoSight for the Measurement of Nanoparticles and Protein Aggregates, *Pharm. Res.*, 2010, **27**(5), 796–810.
30 F. Gottschalk, T. Sonderer, R. W. Scholz and B. Nowack, Modeled Environmental Concentrations of Engineered Nanomaterials(TiO2, ZnO, Ag, CNT, Fullerenes) for Different Regions, *Environ. Sci. Technol.*, 2009, **43**(24), 9216–9222.
31 F. Loosli, J. Wang, S. Rothenberg, M. Bizimis, C. Winkler, O. Borovinskaya, L. Flamigni and M. Baalousha, Sewage spills are a major source of titanium dioxide engineered(nano)-particle release into the environment, *Environ. Sci.: Nano*, 2019, **6**, 763–777.
32 M. Baalousha, M. Sikder, A. Prasad, J. Lead, R. Merrifield and G. T. Chandler, The concentration-dependent behaviour of nanoparticles, *Environ. Chem.*, 2016, **13**(1), 1–3.
33 B. Bocca, F. Petrucci, A. Alimonti and S. Caroli, Traffic-related platinum and rhodium concentrations in the atmosphere of Rome, *J. Environ. Monit.*, 2003, **5**(4), 563–568.
34 J. Schäfer and H. Puchelt, Platinum-Group-Metals(PGM) emitted from automobile catalytic converters and their distribution in roadside soils, *J. Geochem. Explor.*, 1998, **64**(1), 307–314.
35 O. Morton, H. Puchelt, E. Hernández and E. Lounejeva, Traffic-related platinum group elements(PGE) in soils from Mexico City, *J. Geochem. Explor.*, 2001, **72**(3), 223–227.
36 S. Artelt, O. Creutzenberg, H. Kock, K. Levsen, D. Nachtigall, U. Heinrich, T. Rühle and R. Schlögl, Bioavailability of fine dispersed platinum as emitted from automotive catalytic converters: a model study, *Sci. Total Environ.*, 1999, **228**(2), 219–242.
37 C. Barbante, A. Veysseyre, C. Ferrari, K. Van De Velde, C. Morel, G. Capodaglio, P. Cescon, G. Scarponi and C. Boutron, Greenland Snow Evidence of Large Scale Atmospheric Contamination for Platinum, Palladium, and Rhodium, *Environ. Sci. Technol.*, 2001, **35**(5), 835–839.
38 M. Moldovan, S. Rauch, M. Gómez, M. Antonia Palacios and G. M. Morrison, Bioaccumulation of palladium, platinum and rhodium from urban particulates and sediments by the freshwater isopod Asellus aquaticus, *Water Res.*, 2001, **35**(17), 4175–4183.
39 K. Folens, T. Van Acker, E. Bolea-Fernandez, G. Cornelis, F. Vanhaecke, G. Du Laing and S. Rauch, Identification of platinum nanoparticles in road dust leachate by single particle inductively coupled plasma-mass spectrometry, *Sci. Total Environ.*, 2018, **615**, 849–856.
40 K. Ravindra, L. Bencs and R. Van Grieken, Platinum group elements in the environment and their health risk, *Sci. Total Environ.*, 2004, **318**(1), 1–43.
41 J. Pawlak, E. Łodyga-Chruścińska and J. Chrustowicz, Fate of platinum metals in the environment, *J. Trace Elem. Med. Biol.*, 2014, **28**(3), 247–254.
42 K. E. Biesinger and G. M. Christensen, Effects of Various Metals on Survival, Growth, Reproduction, and Metabolism of Daphnia magna, *J. Fish. Res. Board Can.*, 1972, **29**(12), 1691–1700.
43 I. Veltz, F. Arsac, S. Biagianti-Risbourg, F. Habets, H. Lechenault and G. Vernet, Effects of platinum(Pt4+) on Lumbriculus variegatus Muller(Annelida, Oligochaetae): acute toxicity and bioaccumulation, *Arch. Environ. Contam. Toxicol.*, 1996, **31**(1), 63–67.
44 M. Książyk, M. Asztemborska, R. Stęborowski and G. Bystrzejewska-Piotrowska, Toxic Effect of Silver and Platinum Nanoparticles Toward the Freshwater Microalga Pseudokirchneriella subcapitata, *Bull. Environ. Contam. Toxicol.*, 2015, **94**(5), 554–558.
45 C. Wei and G. M. Morrison, Platinum in Road Dusts and Urban River Sediments, *Sci. Total Environ.*, 1994, **146**, 169–174.
46 K. M. Koczkur, S. Mourdikoudis, L. Polavarapu and S. E. Skrabalak, Polyvinylpyrrolidone(PVP) in nanoparticle synthesis, *Dalton Trans.*, 2015, **44**(41), 17883–17905.
47 Gatan Incorporation, in *Gatan Digital Micrograph Software Instalation Instructions*, 2018.
48 G. R. Aiken, D. M. McKnight, K. A. Thorn and E. M. Thurman, Isolation of hydrophilic organic acids from water using nonionic macroporous resins, *Org. Geochem.*, 1992, **18**(4), 567–573.
49 A. M. Graham, G. R. Aiken and C. C. Gilmour, Effect of Dissolved Organic Matter Source and Character on Microbial Hg Methylation in Hg–S–DOM Solutions, *Environ. Sci. Technol.*, 2013, **47**(11), 5746–5754.
50 C. Jiang, B. T. Castellon, C. W. Matson, G. R. Aiken and H. Hsu-Kim, Relative Contributions of Copper Oxide Nanoparticles and Dissolved Copper to Cu Uptake Kinetics

of Gulf Killifish(Fundulus grandis) Embryos, *Environ. Sci. Technol.*, 2017, **51**(3), 1395–1404.

51 B. A. Poulin, J. N. Ryan, K. L. Nagy, A. Stubbins, T. Dittmar, W. Orem, D. P. Krabbenhoft and G. R. Aiken, Spatial Dependence of Reduced Sulfur in Everglades Dissolved Organic Matter Controlled by Sulfate Enrichment, *Environ. Sci. Technol.*, 2017, **51**(7), 3630–3639.

52 N. W. Green, E. M. Perdue, G. R. Aiken, K. D. Butler, H. Chen, T. Dittmar, J. Niggemann and A. Stubbins, An intercomparison of three methods for the large-scale isolation of oceanic dissolved organic matter, *Mar. Chem.*, 2014, **161**, 14–19.

53 E. W. D. Huffman and H. A. Stuber, Analytical methodology for elemental analysis of humic substances, in *Humic Substances in Soil, Sediment, and Water: Geochemistry, Isolation, and Characterization*, Wiley, 1985, pp. 433–456.

54 J. L. Weishaar, G. R. Aiken, B. A. Bergamaschi, M. S. Fram, R. Fujii and K. Mopper, Evaluation of Specific Ultraviolet Absorbance as an Indicator of the Chemical Composition and Reactivity of Dissolved Organic Carbon, *Environ. Sci. Technol.*, 2003, **37**(20), 4702–4708.

55 N. Tolić, Y. Liu, A. Liyu, Y. Shen, M. M. Tfaily, E. B. Kujawinski, K. Longnecker, L.-J. Kuo, E. W. Robinson, L. Paša-Tolić and N. J. Hess, Formularity: Software for Automated Formula Assignment of Natural and Other Organic Matter from Ultrahigh-Resolution Mass Spectra, *Anal. Chem.*, 2017, **89**(23), 12659–12665.

56 M. M. Tfaily, R. K. Chu, N. Tolić, K. M. Roscioli, C. R. Anderton, L. Paša-Tolić, E. W. Robinson and N. J. Hess, Advanced Solvent Based Methods for Molecular Characterization of Soil Organic Matter by High-Resolution Mass Spectrometry, *Anal. Chem.*, 2015, **87**(10), 5206–5215.

57 I. V. Perminova, I. V. Dubinenkov, A. S. Kononikhin, A. I. Konstantinov, A. Y. Zherebker, M. A. Andzhushev, V. A. Lebedev, E. Bulygina, R. M. Holmes, Y. I. Kostyukevich, I. A. Popov and E. N. Nikolaev, Molecular Mapping of Sorbent Selectivities with Respect to Isolation of Arctic Dissolved Organic Matter as Measured by Fourier Transform Mass Spectrometry, *Environ. Sci. Technol.*, 2014, **48**(13), 7461–7468.

58 S. Lee, X. Bi, R. B. Reed, J. F. Ranville, P. Herckes and P. Westerhoff, Nanoparticle Size Detection Limits by Single Particle ICP-MS for 40 Elements, *Environ. Sci. Technol.*, 2014, **48**(17), 10291–10300.

59 R. A. Ploc, Transmission electron microscopy of thin (<2000 å) thermally formed ZrO2 films, *J. Nucl. Mater.*, 1968, **28**(1), 48–60.

60 M. Tejamaya, I. Romer, R. C. Merrifield and J. R. Lead, Stability of Citrate, PVP, and PEG Coated Silver Nanoparticles in Ecotoxicology Media, *Environ. Sci. Technol.*, 2012, **46**(13), 7011–7017.

61 A. M. El Badawy, K. G. Scheckel, M. Suidan and T. Tolaymat, The impact of stabilization mechanism on the aggregation kinetics of silver nanoparticles, *Sci. Total Environ.*, 2012, **429**, 325–331.

62 H. Zhang, J. A. Smith and V. Oyanedel-Craver, The effect of natural water conditions on the anti-bacterial performance and stability of silver nanoparticles capped with different polymers, *Water Res.*, 2012, **46**(3), 691–699.

63 K. A. Huynh and K. L. Chen, Aggregation Kinetics of Citrate and Polyvinylpyrrolidone Coated Silver Nanoparticles in Monovalent and Divalent Electrolyte Solutions, *Environ. Sci. Technol.*, 2011, **45**(13), 5564–5571.

64 S. Lin, Y. Cheng, J. Liu and M. R. Wiesner, Polymeric Coatings on Silver Nanoparticles Hinder Autoaggregation but Enhance Attachment to Uncoated Surfaces, *Langmuir*, 2012, **28**(9), 4178–4186.

65 C. M. Alexander, J. C. Dabrowiak and J. Goodisman, Gravitational sedimentation of gold nanoparticles, *J. Colloid Interface Sci.*, 2013, **396**, 53–62.

66 J. M. Pettibone, D. M. Cwiertny, M. Scherer and V. H. Grassian, Adsorption of Organic Acids on TiO2 Nanoparticles: Effects of pH, Nanoparticle Size, and Nanoparticle Aggregation, *Langmuir*, 2008, **24**(13), 6659–6667.

67 D. P. Stankus, S. E. Lohse, J. E. Hutchison and J. A. Nason, Interactions between Natural Organic Matter and Gold Nanoparticles Stabilized with Different Organic Capping Agents, *Environ. Sci. Technol.*, 2011, **45**(8), 3238–3244.

68 H. Zhang, R. L. Penn, R. J. Hamers and J. F. Banfield, Enhanced Adsorption of Molecules on Surfaces of Nanocrystalline Particles, *J. Phys. Chem. B*, 1999, **103**(22), 4656–4662.

69 Y.-P. Chin, G. Aiken and E. O'Loughlin, Molecular Weight, Polydispersity, and Spectroscopic Properties of Aquatic Humic Substances, *Environ. Sci. Technol.*, 1994, **28**(11), 1853–1858.

70 T. Phenrat, J. E. Song, C. M. Cisneros, D. P. Schoenfelder, R. D. Tilton and G. V. Lowry, Estimating Attachment of Nano- and Submicrometer-particles Coated with Organic Macromolecules in Porous Media: Development of an Empirical Model, *Environ. Sci. Technol.*, 2010, **44**(12), 4531–4538.

71 C. L. Tiller and C. R. O'Melia, Natural organic matter and colloidal stability: Models and measurements, *Colloids Surf., A*, 1993, **73**, 89–102.

72 K.-K. Au, A. C. Penisson, S. Yang and C. R. O'Melia, Natural organic matter at oxide/water interfaces: complexation and conformation, *Geochim. Cosmochim. Acta*, 1999, **63**(19), 2903–2917.

73 M. Baalousha, K. Afshinnia and L. Guo, Natural organic matter composition determines the molecular nature of silver nanomaterial-NOM corona, *Environ. Sci.: Nano*, 2018, **5**(4), 868–881.

74 S. Avneri-Katz, R. B. Young, A. M. McKenna, H. Chen, Y. E. Corilo, T. Polubesova, T. Borch and B. Chefetz, Adsorptive fractionation of dissolved organic matter(DOM) by mineral soil: Macroscale approach and molecular insight, *Org. Geochem.*, 2017, **103**, 113–124.

75 J. A. Davis and R. Gloor, Adsorption of dissolved organics in lake water by aluminum oxide. Effect of molecular weight, *Environ. Sci. Technol.*, 1981, **15**(10), 1223–1229.

76 J. Lv, S. Zhang, S. Wang, L. Luo, D. Cao and P. Christie, Molecular-Scale Investigation with ESI-FT-ICR-MS on

Fractionation of Dissolved Organic Matter Induced by Adsorption on Iron Oxyhydroxides, *Environ. Sci. Technol.*, 2016, **50**(5), 2328–2336.

77 I. Chowdhury, S. L. Walker and S. E. Mylon, Aggregate morphology of nano-TiO2: role of primary particle size, solution chemistry, and organic matter, *Environ. Sci.: Processes Impacts*, 2013, **15**(1), 275–282.

78 Q. Zhou, P. A. Maurice and S. E. Cabaniss, Size fractionation upon adsorption of fulvic acid on goethite: equilibrium and kinetic studies, *Geochim. Cosmochim. Acta*, 2001, **65**(5), 803–812.

79 E. Haslam, *Practical polyphenolics: from structure to molecular recognition and physiological action*, Cambridge University Press, Cambridge, 1998.

80 M. H. Sipponen, H. Lange, M. Ago and C. Crestini, Understanding Lignin Aggregation Processes. A Case Study: Budesonide Entrapment and Stimuli Controlled Release from Lignin Nanoparticles, *ACS Sustainable Chem. Eng.*, 2018, **6**(7), 9342–9351.

81 R. Lal, Mechanisms of Carbon Sequestration in Soil Aggregates AU-Blanco-Canqui, Humberto, *Crit. Rev. Plant Sci.*, 2004, **23**(6), 481–504.

82 T. C. Caesar-TonThat and V. L. Cochran, Soil aggregate stabilization by a saprophytic lignin-decomposing basidiomycete fungus I. Microbiological aspects, *Biol. Fertil. Soils*, 2000, **32**(5), 374–380.

83 C. Xiao, R. Bolton and W. L. Pan, Lignin from rice straw Kraft pulping: Effects on soil aggregation and chemical properties, *Bioresour. Technol.*, 2007, **98**(7), 1482–1488.